

## H<sub>2</sub> OBSERVATIONS OF OUTFLOWS FROM YOUNG STARS

Christopher J. Davis

Joint Astronomy Centre, Hilo, Hawaii, USA.

### RESUMEN

Analizamos observaciones del IR cercano recientes de jets Herbig-Haro (HH) y de flujos moleculares de protoestrellas muy jóvenes profundamente embebidas. Mediciones de movimiento propio y estudios espectroscópicos de baja y de alta resolución muestran la excitación y la cinemática de objetos individuales, que podrían interpretarse en términos de choques de proa de alta velocidad que barren y incorporan material del ambiente para formar flujos moleculares de “CO”. Las propiedades observadas de muchos objetos puede explicarse razonablemente bien con modelos de choques de proa tipo “C” magnetizados, aunque choques del tipo “J” no puede excluirse del todo. Analizamos también nuevas observaciones echelle de las fuentes mismas de los flujos. Estos datos de H<sub>2</sub> muestran emisión de línea de velocidades intermedias y altas en la base del flujo (de menos de unas pocos cientos de unidades astronómicas de la fuente que lo impulsa) en la mayoría de las fuentes observadas. Las propiedades de estas regiones de líneas de emisión de hidrógeno molecular—o MHEL, por sus siglas en inglés—son similares a las regiones de líneas prohibidas (FEL, por sus siglas en inglés) hacia estrellas T Tauri.

### ABSTRACT

Recent near-IR observations of Herbig-Haro (HH) jets and molecular outflows from very young, deeply embedded protostars are discussed. Proper motion measurements, and both low- and high-resolution spectroscopic studies reveal the excitation and kinematics of individual objects, which may be interpreted in terms of high-velocity bow shocks which sweep up and entrain ambient material to form molecular “CO” outflows. The observed properties of many objects can be explained reasonably well with magnetized bow C-shock models, although J-type shocks cannot be ruled out. We also discuss new echelle observations of the outflow sources themselves. These H<sub>2</sub> data reveal intermediate and high-velocity line emission from the base of the outflow (from within a few hundred AU of the driving source) in most of the flows observed. The properties of these “Molecular Hydrogen Emission Line”—or MHEL—regions, are similar to those of Forbidden Emission Line (FEL) regions towards T Tauri stars.

**Key Words:** ISM: HERBIG-HARO OBJECTS — ISM: JETS AND OUTFLOWS — ISM: MOLECULAR HYDROGEN — STARS: PRE-MAIN-SEQUENCE

### 1. INTRODUCTION

We have witnessed in the last five years a rapid improvement in our ability to observe molecular outflows and Herbig-Haro (HH) jets at near-IR wavelengths. As a consequence, our understanding of the excitation and kinematics of individual objects, and the relationship between collimated jets, bow shocks and entrained ambient molecular gas has radically improved. Indeed, we are now able to observe and analyse Herbig-Haro-like shock features in outflows from some of the youngest and most heavily obscured protostars known.

High-resolution images of well-known HH objects in the  $v=1-0$ ,  $J=3-1$  transition of molecular hydrogen (the  $1-0 S(1)$  line) indicate a propensity for curved “bow shock” structures. Typically the H<sub>2</sub>

traces the low-excitation molecular gas excited in the oblique wings of bow shocks, with higher-excitation optical and near-IR forbidden lines being excited nearer the cap of each bow (e.g., Figure 1). The bows themselves are driven by unseen, collimated jets. Cooling instabilities and flow variability probably cause the fragmented structure seen in many HH bow shocks.

### 2. H<sub>2</sub> BOWS AND CO OUTFLOWS: A CAUSAL RELATIONSHIP

There is growing support for the idea that much of the observed “intermediate-velocity” molecular gas (the traditional “CO” outflow; Bachiller 1996) in bipolar outflows is swept up predominantly by molecular bow shocks, the shocks themselves being driven by high-velocity collimated jets or winds.

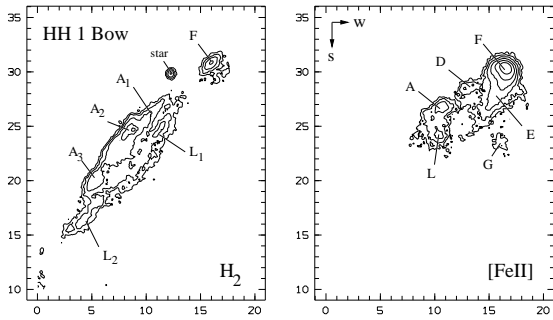


Fig. 1. H<sub>2</sub> and [Fe II] images of HH 1. The emission knots are all moving north-westward at a few hundred km s<sup>-1</sup>. The H<sub>2</sub> is excited in the extended, almost planar shocks associated with the north-eastern edge of the overall structure; the [Fe II] is instead excited near the leading edge of HH 1.

These bows represent the jet-cloud interaction zone, and so are associated with current entrainment activity. The cooling time associated with H<sub>2</sub> in these shocks is very short, of the order of only a few years. Specifically,  $t_c \sim 3 \times 10^8 n_6^{-1} T_3^{-2.3}$  for H<sub>2</sub> densities  $n_6 = n/(10^6 \text{ cm}^{-3}) < 3$ , where  $t_c$  is in seconds and  $T_3$  is the temperature in units of 1000 K (Smith & Brand 1990). Once a jet exits the denser regions of the parental cloud, any associated bow shocks will fade rapidly. However, while still within the cloud, H<sub>2</sub> excitation and ambient gas entrainment will occur.

H<sub>2</sub> images of CO outflows testify to this entrainment process (Davis & Eisloffel 1995). Comparison of H<sub>2</sub> images of molecular bows with recent, high-resolution CO maps of outflows reveal compelling evidence for a causal relationship. The BIMA data of Lee et al. (2000) are particularly insightful (Figure 2), as are published CO and H<sub>2</sub> observations of the high-mass star-forming region W 75N. Note the close correlation between peaks in the CO and H<sub>2</sub> emission in HH 240 (Fig. 2). Similarly, in W 75N the extensive H<sub>2</sub> bow observed to the south-west of the source is seen to envelope the outer, leading edge of the blue-shifted CO outflow lobe (Davis et al. 1998), as one would expect if the lobe represents ambient gas swept up by the H<sub>2</sub> bow shock.

Analytical and numerical simulations of jet-driven flows reproduce with some degree of success the observed characteristics of the bow shocks and CO outflow lobes in W 75N, L 1634 and other regions (Raga & Cabrit 1993; Smith, Suttner, & Yorke 1997; Völker et al. 1999; Downes & Ray 1999; Lee et al. 2000). The models reproduce most of the observed

morphological features, such as the bulge and limb-brightening seen in these and other CO outflows, although the model H<sub>2</sub> bows of Smith et al. tend to exhibit more structure along the flow axis: in W 75N, L 1634, and in many other flows the H<sub>2</sub> emission is usually confined to a thin hemispherical cap with a radius of curvature many times greater than the shock thickness or post-shock cooling length. These jet-driven outflow models also go some way towards explaining observed position-velocity plots, and the slope of the mass-velocity distribution,  $\gamma$ , usually measured across CO outflows ( $\gamma$  is quantified via a simple power-law of the form  $m_v \propto v^{-\gamma}$ ), although opacity at low outflow velocities may effect many of the values reported in the literature (Yu et al. 2000). Also,  $\gamma$  will clearly change along the lobes of each outflow. One would expect the slope of the mass-velocity distribution, and so the value of  $\gamma$ , to *decrease* just behind an advancing shock front and towards the ends of the flow lobes, i.e., at locations in the flow where the ratio of low- to high-velocity gas will be reduced. This does indeed seem to be the case in, for example, the CO  $J=4-3$  map of V380 Ori NE (Davis et al. 2000).

### 3. H<sub>2</sub> EXCITATION ACROSS HH BOWS

Low- and intermediate-resolution near-IR spectroscopy of HH objects and H<sub>2</sub> bow shocks yields useful information about the gas excitation conditions. Although initial studies of a few well-known HH objects suggested a mostly thermal, single-temperature population distribution for H<sub>2</sub> levels with  $v \leq 3$ , a range of excitation temperatures have since been identified in some sources (Schwartz et al. 1995; Everett, DePoy, & Pogge 1995). There may also be a fluorescent contribution to the emission from higher-excitation H<sub>2</sub> lines, due to Ly $\alpha$  pumping of low-density, pre-shock gas (Fernandes & Brand 1995).

To better understand the physics of molecular bow shocks, we need to examine *changes* in excitation across individual shock fronts, as well as along the axes of HH jets and H<sub>2</sub> flows. To this end, we have conducted a detailed study of two molecular bow shocks in two separate outflows, HH 99 and VLA 1623A (HH 313) (Davis et al. 1999). High-resolution H<sub>2</sub> images reveal the well-defined bow shock morphologies of both sources. These we compare to the 2-D magnetohydrodynamic (MHD) models developed by Smith and co-workers (Smith & Brand 1990; Smith 1991; Yu et al. 2000). From the comparison we infer flow inclination angles, shock speeds and the magnetic field in the pre-shock gas in each bow. The same models are then compared

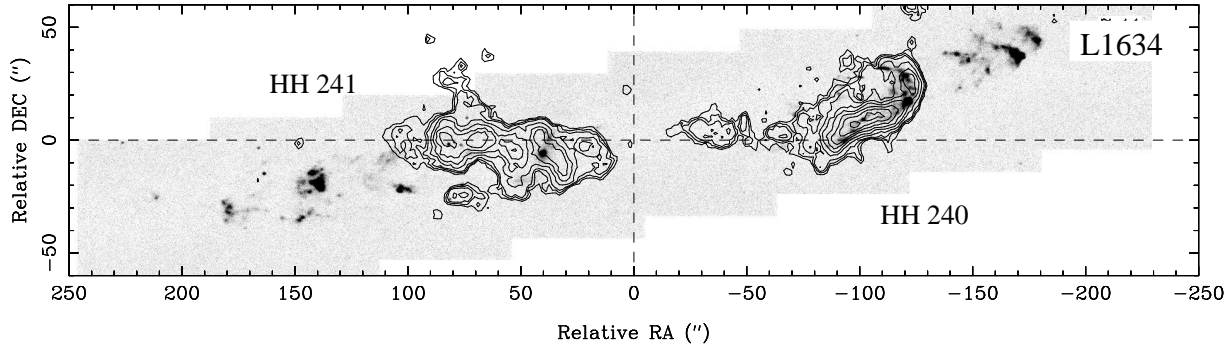


Fig. 2. H<sub>2</sub> 1–0 *S*(1) image of L1634 (HH 240/241) with, superimposed, contours of CO 1–0 emission obtained with the BIMA array (from Lee et al. 2000).

to excitation data. Towards the brighter target, VLA 1623A, we were able to extract spectra at four locations across the bow shock (the slit being orientated along the jet axis). A sample spectrum is shown here in Figure 3.

From the many H<sub>2</sub> ro-vibrational lines in the near-IR bands one can measure column densities for the upper energy levels and then plot *Column Density Ratio*, or CDR diagrams. A CDR plot clearly illustrates departures from single-temperature thermal excitation (which would result in all the points laying on a straight line, the slope of the line being a measure of the excitation temperature). CDR diagrams are described in detail by Burton & Haas (1997) and Eislöffel, Smith & Davis (2000).

Extinction-corrected column densities, derived from three of the four spectra observed across VLA 1623A, are plotted in Figure 4. Superimposed are model CDR curves, predicted by the same bow model used to synthesize the morphological features observed in the H<sub>2</sub> image of VLA 1623A. Kinematic information from the model was also compared to H<sub>2</sub> line profiles observed across the bow surface (see Davis et al. 1999 for details). For the first time, morphology, excitation *and* kinematics are fit with a single bow-shock model. Although only partially successful, we were able to predict (i) the decreasing excitation towards the bow flanks in VLA 1623A (Fig. 4), (ii) intensity distributions that compare very favorably with the high-resolution images of both targets, and (iii) narrow, low-velocity H<sub>2</sub> line profiles similar to those observed.

In a similar study, we (Eislöffel et al. 2000) later examined excitation and kinematic information extracted from intermediate resolution spectra at a number of locations across a further five outflows. As with our earlier study, we found that the data

support a picture in which excitation variations are caused by large-scale shock geometries. The variations are best interpreted with MHD C-shocks, although some locations which demonstrate hydrodynamic J-type excitation were also found. In two targets, the jets themselves were also traced in H<sub>2</sub> emission. We find that the excitation declines with distance from each source. Tedds et al. (these proceedings) likewise discuss changing excitation—from knot to knot—along the axes of three collimated jets, HH 212, HH 111 and HH 46.

#### 4. KINEMATICS OF H<sub>2</sub> BOW SHOCKS

After repeated H<sub>2</sub> imaging campaigns, some groups have taken a first stab at measuring the proper motions of H<sub>2</sub> features in a few outflows. Typically, the tangential velocities match those of optical studies of the same HH objects. This clearly indicates that the H<sub>2</sub> and optical forbidden line emissions derive from the same shock features. However, in some outflows H<sub>2</sub> is excited in different parts of the flow, or in the optically-obscured counterflow. Thus, near-IR proper motion measurements can be complementary to optical kinematic studies.

In HH 46/47, for example, the inferred tangential velocities range from a few tens to almost 500 km s<sup>-1</sup> (Micono et al. 1998). The highest velocities are observed for H<sub>2</sub> knots either in or close to the jet/counterjet axis. Knots constituting the wings of the large scale H<sub>2</sub> bow seen in the counterflow are found to move much more slowly. In HH 111 and HH 121 (see Figure 5) tangential velocities in the range 265–460 km s<sup>-1</sup> are measured (Coppin, Davis, & Micono 1998), while in HH 1 speeds of 150–400 km s<sup>-1</sup> are recorded (Noriega-Crespo et al. 1997). In almost all cases, the tangential velocities exceed the dissociation speed limit for molecular hydrogen in shocks in dense gas; this indicates that the

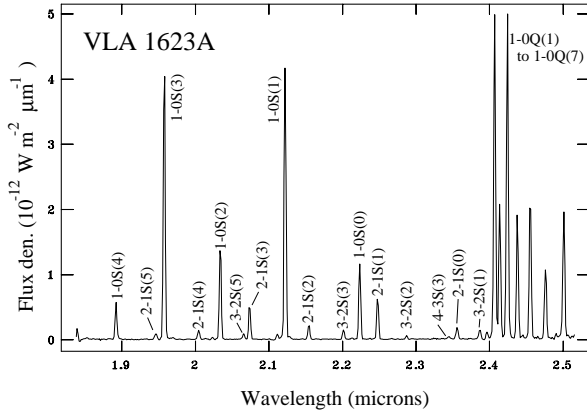


Fig. 3. One of three *K*-band spectra obtained in the HH bow shock VLA 1623A (HH 313).

associated shock velocities are much lower than the shock pattern speeds (the proper motions) and the underlying jet speeds.

Variability of H<sub>2</sub> features were also noted in some outflows. In HH 111 and HH 46/47 several knots significantly changed their luminosity and/or morphology over the 4–5 year timebase used to conduct each study. From these changes a molecular cooling time of the order of a few years is thus inferred, in line with theoretical predictions based on “typical” jet densities and velocities (as noted earlier). More recent proper motion studies for HH 7–11, HH 33/40 and HH 25/26 are discussed by Chrysostomou et al. elsewhere in these proceedings (see also Chrysostomou et al. 2000).

By comparison, H<sub>2</sub> radial velocity measurements are far more common-place (e.g., Carr 1993; Davis & Smith 1996a, 1996b; Tedds et al. 1999; Yu et al. 2000). Typically, H<sub>2</sub> emission lines in HH objects are blue or red shifted by a few tens of km s<sup>-1</sup> from the systemic velocity. Line widths are usually ~ 50 km s<sup>-1</sup> FWHM (although broader lines are evident in the nearby high-mass star forming region OMC-1, Tedds et al. 1999). Lines are often single-peaked and roughly Gaussian in shape, although double-peaked and asymmetric profiles have been observed. In a few H<sub>2</sub> bow shocks double-peaked profiles are detected in the bow flanks. In HH 7, for example, the velocity separation between the low and high-velocity blue-shifted peaks is of the order of 70 km s<sup>-1</sup>, whereas in the HH 72B and L 1551-IRS5 bow shocks we observe a peak-to-peak separation that is considerably larger, approaching 150 km s<sup>-1</sup> (Davis et al. 2001). Double-peaked profiles are expected in hollow, shell-like bow shocks,

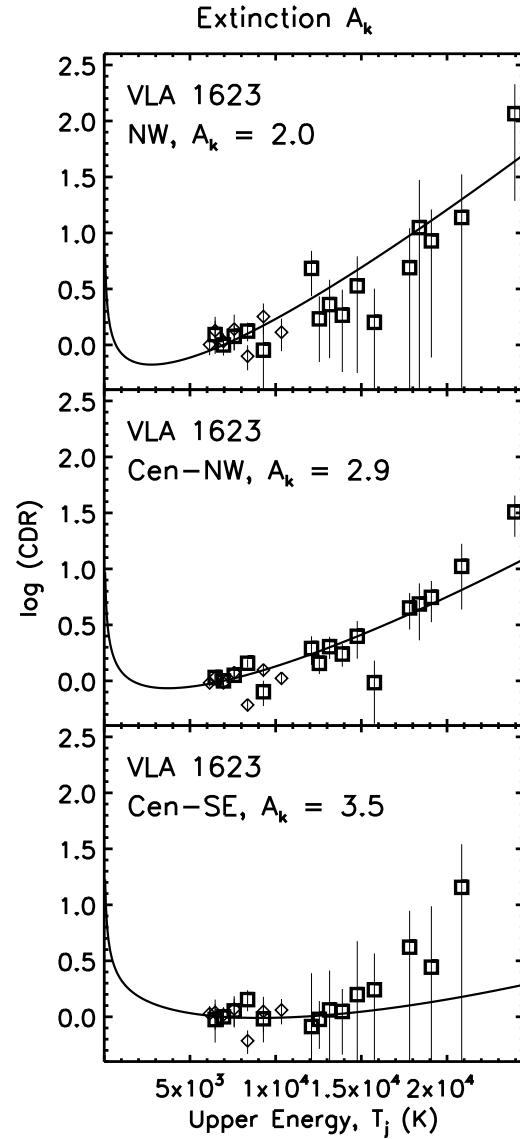


Fig. 4. Comparison of model CDR curves to (extinction-corrected) H<sub>2</sub> column densities derived from spectra obtained at three positions across VLA 1623A. Only the *K*-band data are used. Data at locations near the bow head (top), near the bow center (middle) and towards the bow flanks (bottom) are plotted. The solid lines are CDR curves predicted by the same model used to synthesize the observed morphology and luminosity of the bow shock; they are *not* fits to the data. The same MHD models are also used to predict H<sub>2</sub> profiles, for comparison with H<sub>2</sub> echelle observations. See Davis et al. (1999) for details.

where emission is excited in the near and far sides of the bow shock shell. In these three examples, the

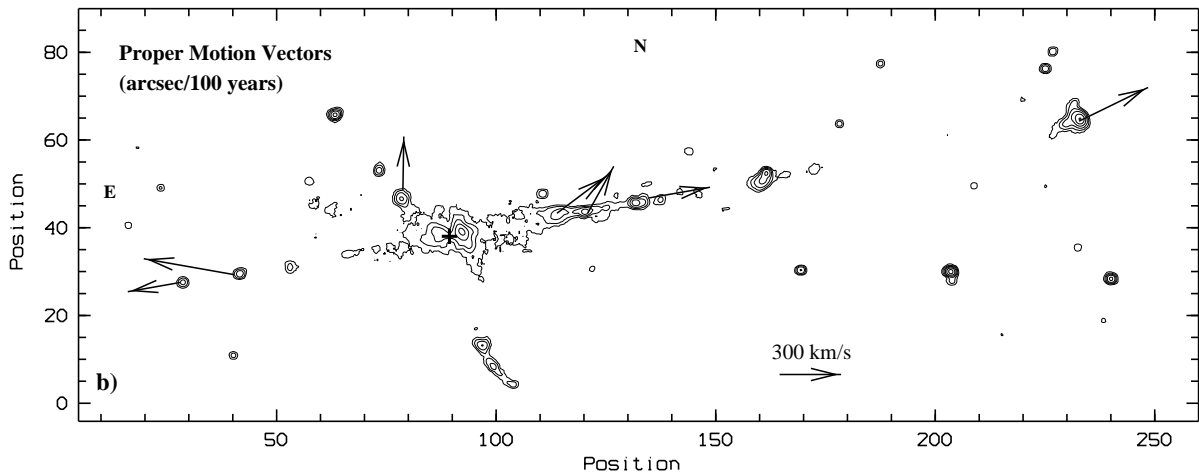


Fig. 5. Proper motions of H<sub>2</sub> knots in HH 111 and HH 121 (Coppin et al. 1998).

low-velocity component is brighter than the high-velocity peak, which would be consistent with a high-velocity “bullet” interpretation, rather than a “shocked stationary clump” model (e.g., Hartigan et al. 1987). However, the peak-to-peak separations, and the overall velocity extent of the emission lines, are remarkably high.

Models of line profiles from unresolved bow shocks predict that the Full-Width at Zero Intensity (FWZI) extent of the lines should be equivalent to the overall bow shock velocity (Hartigan et al. 1987). However, this analytical treatment assumes that emission comes from all parts of the bow shock. In fast molecular bows H<sub>2</sub> will be dissociated near the head of the bow, where shock speeds (normal to the shock surface) exceed the molecular dissociation “speed limit”,  $v_d$ , which is of the order of  $\sim 50 \text{ km s}^{-1}$  in magnetic C-shocks, unless the magnetic field is extremely high (Smith 1994) or the preshock density low. The maximum velocity dispersion from a planar shock is therefore limited to  $v_d$ . If the flow is orientated close to the plane of the sky, then the *maximum* FWZI velocity dispersion measurable in H<sub>2</sub> from a bow is given by  $\Delta V_{\text{FWZI}} = 2v_d \sin \theta \cos \alpha_d$ , where  $\theta$  is the orientation angle of the flow with respect to the line of sight and  $\alpha_d = \sin^{-1}(v_d/v_s)$  is the maximum angle between the shock plane and the bow shock direction for which H<sub>2</sub> survives to be excited, in which  $v_s$  is the bow shock velocity along the flow axis.<sup>1</sup>

<sup>1</sup>Note that this may be different from the velocity of the bow with respect to the “stationary” source, since the knots in a jet may be internal shocks that impact moving jet gas ahead of them.

The quantity  $\Delta V_{\text{FWZI}}$  is strongly dependent on  $v_d$ ; indeed, the FWZI velocity dispersion should never exceed  $2v_d \sim 100 \text{ km s}^{-1}$ . This does seem to be the case in many outflows, though not in all. For example, the double-peaked profiles noted earlier (in HH 72B and L 1551-IRS5) are somewhat broader. The overall profile shapes may therefore not simply be the result of bow shock geometry. Instead, the low and high-velocity components may represent emission from bow shock gas and jet material, respectively. The low-velocity component could be radiating from precursor gas just ahead of an advancing C-type bow shock; this would explain the low peak velocity and broad line profiles. The high-velocity gas could then be excited in the jet flow, perhaps in the Mach disk, although this would require a molecular component to the underlying jet. Note that we do see the low-velocity component extending further ahead (downwind) of the high-velocity H<sub>2</sub>—at least in the three examples considered here—which would be expected of such a scenario.

## 5. H<sub>2</sub> EMISSION FROM THE BASE OF YSO JETS—“MHEL” REGIONS REVEALED.

In addition to the high-velocity H<sub>2</sub> observed in the extended lobes of HH jets and molecular outflows (discussed in the previous section), H<sub>2</sub> has also been detected towards a number of outflow sources (Greene & Lada 1996; Reipurth & Aspin 1997). We have recently examined the properties of these emission regions via echelle spectroscopy observations of nine outflow sources (Davis et al. 2001). H<sub>2</sub> and Br $\gamma$  observations were obtained towards each Class I source, with the spectrometer slit orientated along

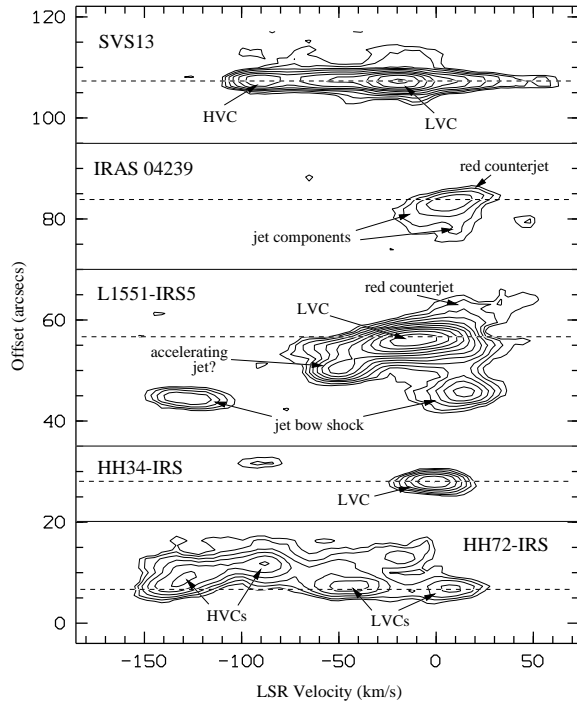


Fig. 6. H<sub>2</sub> Position-Velocity plots towards Class I HH energy sources. The continuum emission from each source (marked with a dashed line) has been removed to leave only the line emission associated with each MHEL region.

the flow axis in each case. Br $\gamma$  and/or H<sub>2</sub> was detected towards most of the sources. However, we found a number of distinct differences between the H<sub>2</sub> and Br $\gamma$  results. The Br $\gamma$  profiles are much wider than their H<sub>2</sub> counterparts, although the H<sub>2</sub> profiles are, in a few cases at least, more structured (less Gaussian). Also, in all cases the Br $\gamma$  emission is confined to the outflow source, being unresolved along the slit/outflow direction, whereas the H<sub>2</sub> is extended along the flow axis, even towards sources where H<sub>2</sub> is detected only towards the source position.

To better illustrate the extended H<sub>2</sub> regions we plot in Figure 6 contour diagrams of five outflow source regions. The continuum emission associated with each YSO has been fitted and removed, row-by-row via linear least-squares fits to the emission on either side of the H<sub>2</sub> line-emission peaks, so that only the line emission remains. Multiple velocity components are revealed in most sources (described in detail by Davis et al. 2001). Also, from Gaussian fits to the H<sub>2</sub> emission peaks and continuum strips either side of the H<sub>2</sub> regions we were able to measure the

spatial offsets of the H<sub>2</sub> components from the continuum position. In four of the five sources shown here we found clear offsets of the H<sub>2</sub> emission, by a few tenths of an arcsecond, from the driving YSO (there was no measurable offset in HH 34-IRS). Moreover, in individual objects, the offset was found to increase at higher blue-shifted velocities.

HI profiles have been observed in a large number of classical T Tauri stars (e.g., Hartmann, Hewett & Calvet 1994; Folha & Emerson 2001). Line shapes are typically interpreted in terms of magnetospheric accretion (Muzerolle, Calvet, & Hartmann 1998), although the profiles may also be modified by outflow processes. The Br $\gamma$  profiles observed towards the Class I sources in our survey are probably produced in the same way. The H<sub>2</sub> emission is, on the other hand, almost certainly associated with the outflow in each system, since it is extended along the outflow axis and in most cases offset from the outflow position (by a few tenths of an arcsecond, or a few hundred AU). Indeed, the properties of these H<sub>2</sub> line emission regions, observed in our sample of Class I outflow sources, are very similar to those of *Forbidden Emission-Line* (FEL) regions observed in many classical T Tauri stars (Hartigan, Edwards, & Ghandour 1995; Hirth, Mundt, & Solf 1997). Consequently, we refer to these regions as *Molecular Hydrogen Emission Line*, or MHEL, regions.

A number of theories have been presented to explain the FEL regions observed in TTSs (e.g., Kwan & Tadamaru 1995; Ouyed & Pudritz 1994). These models may also explain the MHEL regions observed towards the younger, Class I outflow sources. For FELs, a model that assumes two independent flow components is preferred (Hirth et al. 1997), since this accounts for the different excitation conditions observed in low and high-velocity components in FELs. Kwan (1997) suggests that while the high-velocity component (HVC) probably derives from a collimated, high-velocity jet, the low-velocity component (LVC) could be produced in a warm disk corona or a slow disk wind.

Typically the MHEL line profile widths measure 60–160 km s<sup>-1</sup> (FWZI). Such line broadening could be due to Keplerian rotation in or near the accretion disk surface (Hartigan et al. 1995), or simply through lateral expansion of the outflowing gas (Hamann 1994). If the former applies, then the FWZI of each H<sub>2</sub> profile should reflect the maximum velocity attained in the inner regions of the accretion disk. Given the inclination angle of the flow to the line of sight,  $\theta$ , one may estimate the maximum Keplerian velocity associated with the H<sub>2</sub> and Br $\gamma$  emission re-

gions, since  $V_{\text{kep}} = \Delta V_{\text{FWZI}} / (2 \sin \theta)$ . The narrow  $\text{H}_2$  profiles obviously lead to a much lower velocity than the  $\text{Br}\gamma$  observations. Since  $V_{\text{kep}}^2$  is inversely related to the radial distance of the emitting “ring”, it is not surprising that the higher-excitation  $\text{Br}\gamma$  emission would derive from much closer in to the star. Indeed, for a  $1 M_{\odot}$  star, a typical broadened  $\text{Br}\gamma$  profile with  $V_{\text{kep}} \sim 250 \text{ km s}^{-1}$  could originate from a ring of radius  $\sim 2 \times 10^{11} \text{ cm}$ ; the  $\text{H}_2$  would then arise from further out in the disk plane, at a radius of  $\sim 9 \times 10^{12} \text{ cm}$  for a Keplerian velocity of  $40 \text{ km s}^{-1}$ .

Since the MHEL regions are almost certainly associated with each outflow, the  $\text{H}_2$  profiles could instead be broadened by expansion of the flow lobe. Taking into account the inclination angle of the flow axis,  $\theta$ , the flow opening angle,  $\alpha = 2.0 \arctan(\Delta V_{\text{FWZI}} \cos \theta / 2V_{\text{peak}})$ , where  $V_{\text{peak}}$  is the velocity of the HVC or LVC emission peak. For “typical” values of  $\Delta V_{\text{FWZI}} \sim 70 \text{ km s}^{-1}$  and  $\theta \sim 45^\circ$  the full opening angle of an LVC with  $V_{\text{peak}} \sim 20 \text{ km s}^{-1}$  would be roughly  $100^\circ$ ; by comparison, an HVC with a similar FWZI though a  $V_{\text{peak}} \sim 70 \text{ km s}^{-1}$  would have an opening angle of the order of  $40^\circ$ . These very crude values are likely to be overestimated, since turbulence and thermal motions will contribute to the line broadening. The observations, particularly of SVS 13 where both LVC and HVC components are detected in  $\text{H}_2$  (Fig. 6), do nevertheless indicate that the HVC is probably more highly collimated than the LVC, as is the case with optical FEL regions.

## REFERENCES

Bachiller, R. 1996, *ARA&A*, 34, 111  
 Burton, M. G., & Haas, M. R. 1997, *A&A*, 327, 309  
 Carr, J. S. 1993, *ApJ*, 406, 553  
 Chrysostomou, A., Hobson, J., Davis, C. J., Smith, M. D., & Berndsen, A., 2000, *MNRAS*, 314, 229  
 Coppin, K. E. K., Davis, C. J., & Micono, M. 1998, *MNRAS*, 301, L10  
 Davis, C. J., Dent, W. R. F., Matthews, H. E., Coulson, I. M., & McCaughrean M. J. 2000, *MNRAS* 318, 952  
 Davis, C. J., & Eisloffel, J. 1995, *A&A*, 300, 851 (Erratum: *A&A*, 305, 694)  
 Davis, C. J., Ray, T. P., Desroches, L., & Aspin, C. 2001, *MNRAS*, 326, 524  
 Davis, C. J., & Smith, M. D. 1996a, *A&A*, 309, 929

\_\_\_\_\_. 1996b, *A&A*, 310, 961  
 Davis, C. J., Smith, M. D., Eisloffel, J., & Davies, J. K. 1999, *MNRAS*, 308, 539  
 Davis, C. J., Smith, M. D., & Moriarty-Schieven, G. H. 1998, *MNRAS*, 299, 825  
 Downes, T. P., & Ray, T. P. 1999, *A&A*, 345, 977  
 Eisloffel, J., Smith, M. D., & Davis, C. J. 2000, *A&A*, 359, 1147  
 Everett, M. E., DePoy, D. L., & Pogge, R. W. 1995, *AJ*, 110, 1295  
 Fernandes, A. J. L., & Brand, P. W. J. L. 1995, *MNRAS*, 274, 639  
 Folha, D. F. M. & Emerson, J. P. 2001, *A&A*, 365, 90  
 Greene, T. P., & Lada, C. J. 1996, *AJ*, 112, 2184  
 Hamann, F. 1994, *ApJS*, 93, 485  
 Hartigan, P., Edwards, S., & Ghandour, L. 1995, *ApJ* 452, 736  
 Hartigan, P., Raymond, J. C., & Hartmann, L. 1987, *ApJ*, 316, 323  
 Hartmann, L., Hewett, R., & Calvet, S. 1994, *ApJ*, 426, 669  
 Hirth, G., Mundt, R., & Solf, J. 1997, *A&AS*, 126, 437  
 Kwan, J. 1997, *ApJ*, 489, 284  
 Kwan, J., & Tadamaru, E. 1995, *ApJ*, 454, 382  
 Lee, C. F., Mundy, L. G., Reipurth, B., Ostriker, E. C., & Stone, J. M. 2000, *ApJ*, 542, 925  
 Micono, M., Davis, C. J., Ray, T. P., Eisloffel, J., & Shetrone, M. D. 1998, *ApJ*, 494, L227  
 Muzerolle, J., Calvet, N., & Hartmann, L. 1998a, *ApJ*, 116, 2965  
 Noriega-Crespo, A., Garnavich, P. M., Curiel, S., Raga, A. C., & Ayala, S. 1997, *ApJ*, 486, L55  
 Ouyed, R., & Pudritz, R. E. 1994, *ApJ*, 423, 753  
 Raga, A. C., & Cabrit, S. 1993, *A&A*, 278, 267  
 Reipurth, B., & Aspin, C. 1997, *AJ*, 114, 2700  
 Schwartz, R. D., Schultz, A. S. B., Cohen, M., & Williams, P. M. 1995, *ApJ*, 446, 318  
 Smith, M. D. 1991, *MNRAS*, 252, 378  
 Smith, M. D. & Brand, P. W. J. L. 1990, *MNRAS*, 243, 498  
 \_\_\_\_\_. 1994, *MNRAS*, 266, 238  
 Smith, M. D., Suttner, G., & Yorke, H. W. 1997a, *A&A*, 323, 223  
 Tedds, J. A., Brand, P. W. J. L., & Burton, M. G. 1999, *MNRAS*, 307, 337  
 Völker, R., Smith, M. D., Suttner, G., & Yorke, H. W. 1999, *A&A*, 343, 953  
 Yu, K. C., Billawala, Y., Smith, M. D., Bally, J., & Butner, H. M. 2000, *AJ*, 120, 1974